Proceedings of the Institution of Mechanical Engineers, Part G: Journal of Aerospace Engineering
http://pig.sagepub.com/

Aerodynamic study of the dart paper airplane for micro air vehicle application

Jörg U. Schlüter

Proceedings of the Institution of Mechanical Engineers, Part G: Journal of Aerospace Engineering published online 1 March 2013
DOI: 10.1177/0954410013476778

The online version of this article can be found at:
http://pig.sagepub.com/content/early/2013/02/27/0954410013476778

Published by:
SAGE
http://www.sagepublications.com

On behalf of:
Institution of Mechanical Engineers
Institution of MECHANICAL ENGINEERS

Additional services and information for *Proceedings of the Institution of Mechanical Engineers, Part G: Journal of Aerospace Engineering* can be found at:

Email Alerts: http://pig.sagepub.com/cgi/alerts

Subscriptions: http://pig.sagepub.com/subscriptions

Reprints: http://www.sagepub.com/journalsReprints.nav

Permissions: http://www.sagepub.com/journalsPermissions.nav

>> OnlineFirst Version of Record - Mar 1, 2013

What is This?

Downloaded from pig.sagepub.com at University of Sydney on March 4, 2013

Original Article

Institution of MECHANICAL ENGINEERS

Journal of AEROSPACE ENGINEERING

Proc IMechE Part G:
J Aerospace Engineering
0(0) 1–10
© IMechE 2013
Reprints and permissions:
sagepub.co.uk/journalsPermissions.nav
DOI: 10.1177/0954410013476778
uk.sagepub.com/jaero

SAGE

Aerodynamic study of the dart paper airplane for micro air vehicle application

Jörg U Schlüter

Abstract

The aerodynamic design of micro air vehicles is challenging since previous studies have shown that the aerodynamic efficiency of airfoils and wings decreases substantially at low Reynolds-numbers. While many MAV approaches investigate biological designs, here a study is conducted on the aerodynamics of paper airplanes, which fly in the same Reynolds-number range as MAV, but have the advantage of simplicity compared to biological counterparts. Flow visualizations and force measurements in a water tunnel as well as large-eddy simulations are presented on one of the simplest paper airplane design: the dart. The results show that the high-sweep delta design of such an airplane provides high lift coefficients at low Reynolds-numbers. Furthermore, the centerfold of the airplane as a mean to improve the aerodynamic performance is identified.

Keywords

Micro air vehicles, delta wings, low Reynolds-number flows

Date received: 18 June 2012; accepted: 15 November 2012

Introduction

Paper airplanes are a source of inspiration for all ages and have been the introduction to aeronautical engineering for many generations. The fascination of these airplanes has led to a wide variety of paper airplane designs that stem from countless hours of experimentation. As such, the designs of the paper airplanes have been optimized by trial-and-error through a large number of design cycles. Similar to the biological evolutionary process, the most popular designs have shown to be the most performing and the simplest to manufacture.

The current push to design micro air vehicles (MAV) struggles with the inherently limited aerodynamic performance of airfoils and wings at low Reynolds-numbers.[1] For example, wings at $\mathrm{Re} = 70{,}000$ have difficulties to attain lift coefficients larger than $C_{L,max} > 0.75$[2]. Many approaches to overcome this limitation attempt to mimic nature and use some variation of flapping wings[3,4]. However, biological designs are inherently difficult to copy, as the structure and control of an avian wing is highly complex.

In the field of fixed-wing MAV, several working designs exist, such as the Naval Research Lab (NRL) micro tactical expendable (MITE)[5] and the black widow.[6] However, to create sufficient lift, these require relatively high airspeeds (30 km/h and 50 km/h, respectively) that prohibit their use in closed environments.

As such, aircraft designs are sought that are able to provide high lift coefficients, even at low Reynolds-numbers. Attempts to increase the lift coefficients at low Reynolds-numbers by airfoil shaping,[7] passive flaps[8] and gurney flaps[9,10] have been conducted with considerable success, but have limited effect on the overall lift coefficient of the vehicle due to the inherently low aspect ratios of MAV.

Paper airplanes can provide inspirations to improve MAV designs. For example, it is interesting to note that the majority of paper airplane designs are using some variation of a delta wing. Previous studies showed that the aerodynamic performance of delta wing designs with sharp leading edges are relatively unaffected by Reynolds-number effects.[11] In the context of MAV, current research concentrates on delta wings with low-sweep angles,[12,13] presumably to avoid low aspect ratios. However, since most paper airplane designs have high-sweep angles, this current study directs its attention to this kind of design. A recent

School of Mechanical and Aerospace Engineering, Nanyang Technological University, Singapore

Corresponding author:
Jörg U Schlüter, Nanyang Technological University, School of Mechanical and Aerospace Engineering, 50, Nanyang Avenue, Singapore, 639798, Singapore.
E-mail: schluter@ntu.edu.sg

Downloaded from pig.sagepub.com at University of Sydney on March 4, 2013

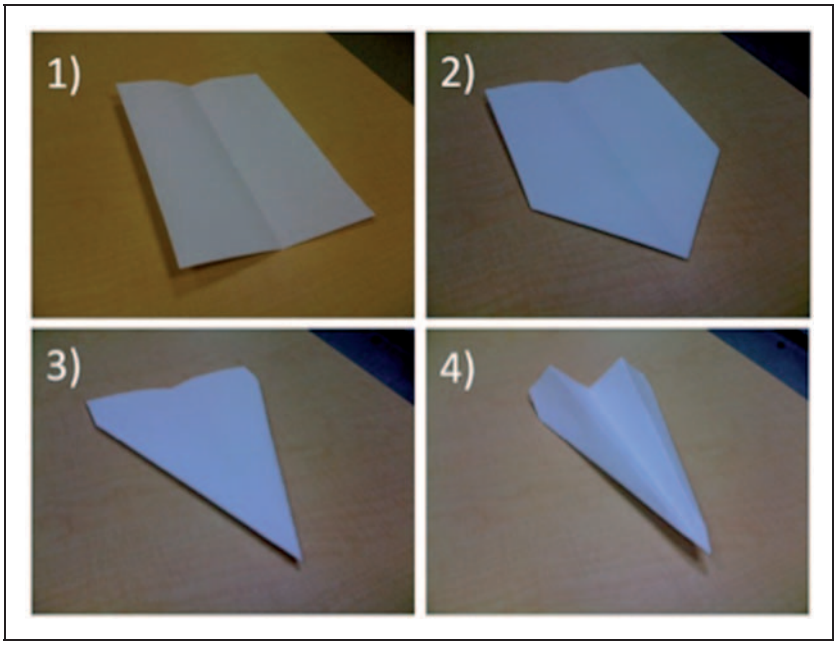

Figure 1. Folding procedure to obtain dart paper airplane.

study of paper airplanes indicated that the centerfold of the paper airplane has a modest influence on the lift of the aircraft.[14]

The distinguishing feature of the flow over a delta wing is the wing vortex, which is formed on the upper side of the delta wing and extends along the entire length of the wing. The low pressure within the vortex contributes to the pressure difference and the lift generated. Furthermore, the vortex re-energizes the boundary layer and allows the production of lift at very high angles of attack. Vortices have been used to increase the lift of MAV mainly in the context of the leading edge vortex (LEV).[15–20] While the LEV produces very high lift, it does so only for a limited time as it is an unsteady effect, and furthermore, the LEV requires an actuation mechanism to perform the flapping motion. The advantage of the delta wing is that it can produce such a vortex in a continuous manner, albeit at a reduced strength.

The current study would like to determine whether designs similar to paper airplanes do have an advantage over conventional designs. If so, a future MAV design based on the geometrical parameters of a paper airplane can be envisioned, in particular, since the manufacturing of such an MAV would be relatively simple. To quantify the aerodynamic performance of such a design, water tunnel experiments and large-eddy simulations (LES) of a dart paper airplane are conducted to determine the suitability of high-sweep delta wing designs for MAV and to determine the effect of the centerfold on those designs. The study would like to show that lift coefficients for these geometries are sufficiently high to produce lift for a compact MAV. Furthermore, the significance of the centerfold on the aerodynamic performance is examined, as this has not been subject of previous investigations.

Water tunnel measurements

Experimental setup

Here, one of the most common airplane designs will be studied: the dart, as it is one of the best examples of a paper airplane design based on a delta wing.

The dart design can be achieved by folding a piece of paper along the centerline of the long side (Figure 1). The corners are then folded outwards thrice. At the wing tips, winglets can be folded up. Based on an A4 sized paper sheet, the airplane has a wingspan of $b = 160\,\text{mm}$ and a wing area of $S = 20{,}000\ \text{mm}^2$, leading to a rather low aspect ratio of $AR = 1.28$. The sweep angle is $\Lambda = 75^\circ$.

For force measurements and numerical analysis, the geometry is simplified by removing the tip of the airplane (Figure 2). This facilitates meshing and numerical convergence as triangular geometries are notoriously difficult to mesh using structured meshes and the stagnation point on the pointed tip is a location of very high pressure gradients that need to be resolved. The removal of the tip alleviates these issues significantly.

A water tunnel is used for flow visualizations and the measurement of lift (Figure 3). The water tunnel is a model of the LongWin Science and Technology Corporation Pte. Ltd. with a contraction ratio of 1:6 and a test section size of 0.3 m wide $\times$ 0.3 m high $\times$ 1.0 m long. The flow uniformity is 1% or better, and the turbulence intensity at the flow speeds used

Downloaded from pig.sagepub.com at University of Sydney on March 4, 2013

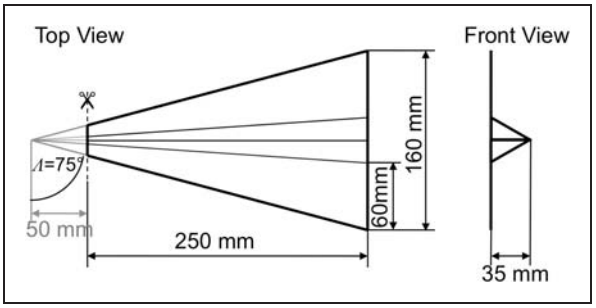

Figure 2. Geometry of the simplified dart paper airplane design.

Figure 3. Water tunnel.

in this study is below 1%, both measured with a Dantec MiniCTA hotfilm anemometer.

Forces are measured with an external three-component force balance (Figure 4) from PT Chroma International Pte. Ltd. measuring lift and drag using the same setup as earlier investigations.[8] The accuracy of the load cells is given by the manufacturer as 0.5% of the full load of 20 N, which translates into a maximum absolute error of 0.1 N.

First, flow visualizations are carried out to characterize the flow field qualitatively. The model for the flow visualization is that of the original dart design made from folded aluminum of 1 mm strength.

To determine the effect of the centerfold on the aerodynamic performance quantitatively, two variations of the simplified model have been studied (Figure 5):

(a) The dart design with a centerfold (Model 1);
(b) A flat delta wing with the trapezoidal planform of the dart design (Model 2).

The models are manufactured from folded aluminum of 0.8 mm strength and scaled 1:2 compared to a paper airplane. In order to maintain Reynolds similarity in the water tunnel, the flow speed is adjusted to 0.6 m/s in water corresponding to a flight speed of about 5 m/s in air as measured in

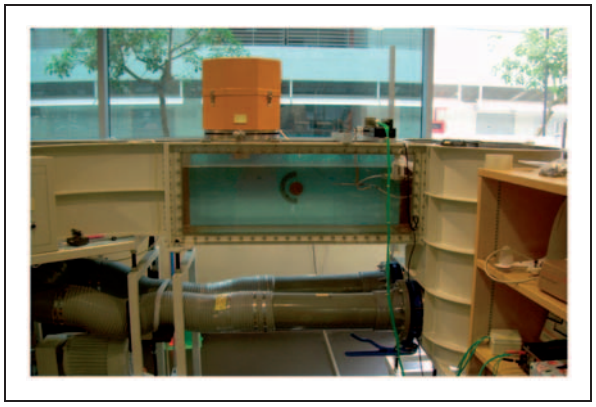

Figure 4. Water tunnel test section with three component balance.[14]

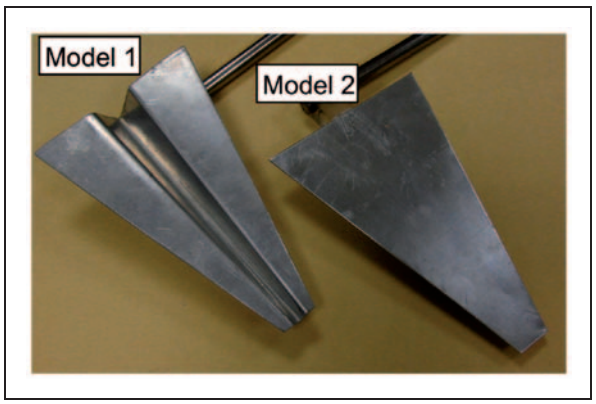

Figure 5. Water tunnel force measurements models with centerfold (Model 1) and without centerfold (Model 2).

an earlier study as the approximate speed of a paper airplane.[14]

Flow visualization

Food dye is used to visualize the main flow features around the paper airplane. As mentioned earlier, one of the major flow features of a delta wing is the vortex on the upper side of the wing.

Figure 6 shows the flow visualization of that wing vortex at a Reynolds-number of Re = 55,000. The dye is injected on the edge of the lower side of the wing at a distance of one-third of the airplanes length downstream of the tip. The wing vortex is also observable at higher Reynolds-numbers, but difficult to visualize and present in still images.

The main difference of the dart paper airplane and a traditional delta wing is the centerfold. While the centerfold has a number of operational advantages, such as providing a handle for launch and increasing its lateral stability, the study here is to assess its influence on the main wing flow. When injecting dye close to the centerfold, the streamlines have a distinct component toward the center (Figure 7). Since the

Downloaded from pig.sagepub.com at University of Sydney on March 4, 2013

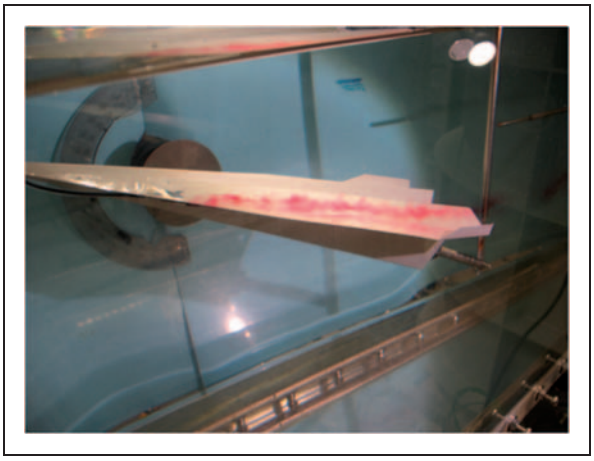

Figure 6. Wing vortex at high angles of attack (Re = 55,000).[14]

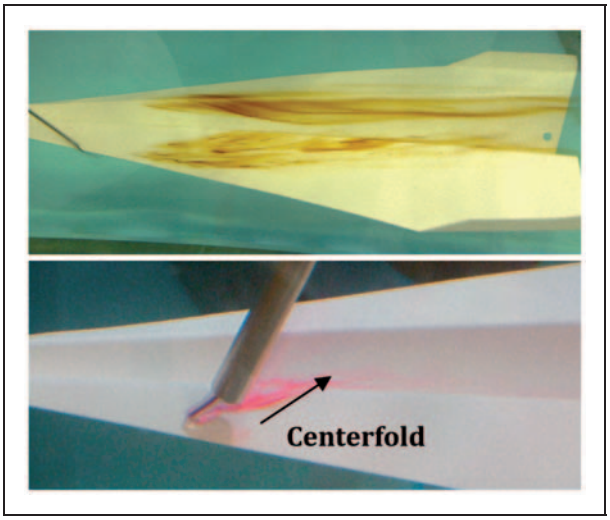

Figure 7. Streamlines close to the centerfold.[14]

centerfold opens up toward the tail, the mass flow rate inside the centerfold increases from its tip toward the tail. As such, it draws mass from the main wing toward the center.

In order to assess the influence of the centerfold onto the wing vortex, the centerfold was covered with clear tape. Figure 8 compares the flow visualizations of the model with a covered and open centerfold. It can be observed that the vortex is drawn slightly more toward the center of the airplane by the flow into the centerfold.

Lift measurements

To quantify the aerodynamic performance of a dart paper airplane and to determine the effect of the centerfold, force measurements were conducted.

First, to assess the accuracy of the experimental setup, Figure 9 shows the lift curve measured for the trapezoidal delta wing (Model 2) in comparison with literature data of Traub et al. and Wentz and Kohlman. Traub et al. measured the lift curve of a delta wing with a sweep angle of $\Lambda = 70^\circ$ at a Reynolds-number of Re = 60,000. Wentz and Kohlman used the same geometry at a higher

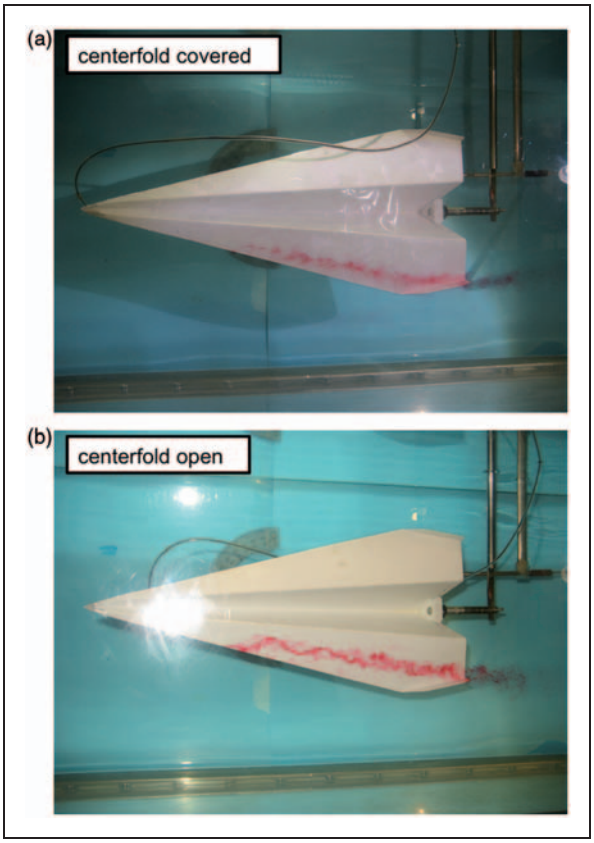

Figure 8. Comparison of wing vortex trajectory (Re = 28,000): (a) centerfold covered with clear tape and (b) original model.[14]

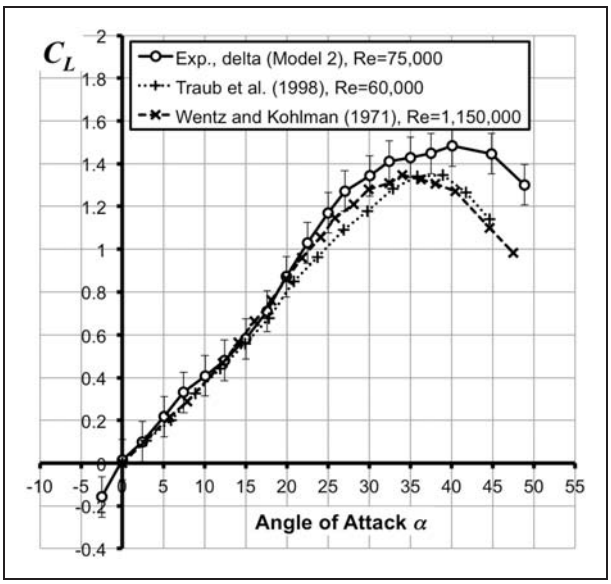

Figure 9. Lift-curve of the delta wing (Model 2) compared to literature data.

Downloaded from pig.sagepub.com at University of Sydney on March 4, 2013

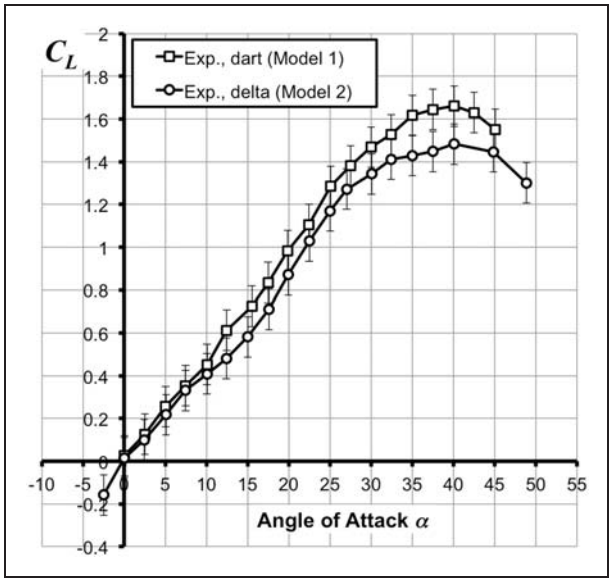

Figure 10. Comparison water tunnel measurements of model with (Model 1) and without centerfold (Model 2).

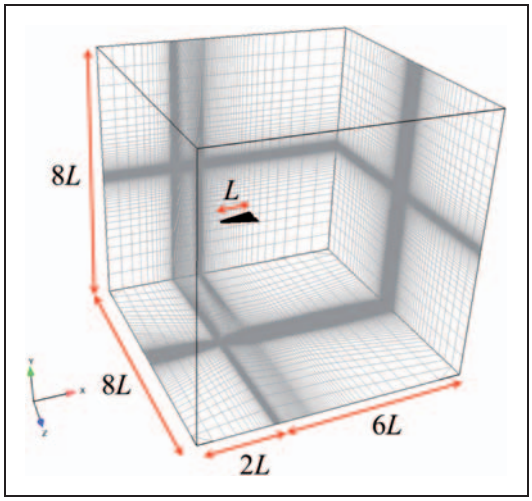

Figure 11. Computational domain of the simulation in terms of the length L of the airplane.

Reynolds-number. As can be seen from the measurements, the influence of the Reynolds-number on the aerodynamic lift force coefficient of the sharp edged delta wings is minimal. The agreement between the current measurements and the literature data is good, with the exception of very high angles of attack. The disagreement at high angles of attack can be explained by the wall effect, which are not corrected for in our measurements. In order to assess the accuracy of the force measurements, the error bars denoting the maximum error of the balance readings are added.

Figure 10 compares the lift curve for the two models, with and without centerfold. The experimental data shows that the presence of the centerfold results in a modest increase of lift. The error bars on both curves show again the maximum error of the balance. However, the measured increase is in the same order of magnitude as the accuracy of the balance. Hence, additional numerical studies of these geometries were conducted.

Large-eddy simulations

Numerical setup

To support the experimental findings, LES were performed to ascertain that the measured increase in lift is not due to experimental errors. An LES approach is used for the simulation of the low Reynolds-number delta wings, since its inherently unsteady formulation is a better choice for the unsteady effects observed in delta wing aerodynamics.[21,22]

The solver used for this investigation is the CDP solver version 2.3 developed at the Center for Turbulence Research at Stanford University. The code solves the filtered continuity and momentum equations on an unstructured mesh.[23,24] The filtered momentum equations are solved on a cell-centered unstructured mesh and are second order accurate. An implicit time-advancement is applied. A dynamic model for the subgrid stresses is employed.[25]

The mesh is a structured grid with 1.6 million mesh elements (Figure 11). With L being the length of the aircraft, the domain extends $2L$ upstream, $6L$ downstream and $4L$ in all lateral directions. The upstream and bottom plane of the domain are defined as inflow planes, the sides are defined as slip walls and the upper and downstream side as convective outlets.

The wall distance of the first mesh cell is at a maximum of $y^+ < 11$. While the y^+ is not particularly low, in this simulation, it is especially important to resolve the wing vortex well, as the pressure difference arising from the presence of the vortex core dominates the drag force. The sharp leading edge of the geometry is the origin of the vortex roll-up and is not dependent of the nature of the boundary layer. This can be seen, for example, by the fact that the lift and drag of a delta wing is independent of the Reynolds-number of the flow, meaning that it is not important, whether the boundary layer is laminar, transitional or turbulent. Hence, the mesh resolution concentrates on the resolution of the wing vortex. The mesh resolution above the upper surface is especially high as the vortex breakdown requires a sufficiently closely spaced mesh.[26–28] To demonstrate mesh independency, one case was run with 3.8 million cells and a $y^+ < 6$ at an angle of attack of $\alpha = 20^\circ$ and the lift and drag force differed less than 4% from the coarse mesh results.

All simulations are run for 10 flow-through times to establish a fully developed flow with statistically steady state conditions and then the data are averaged over another 10 flow-through times, where the flow-through time is defined as the time the flow needs to travel with the freestream velocity over the length of

Downloaded from pig.sagepub.com at University of Sydney on March 4, 2013

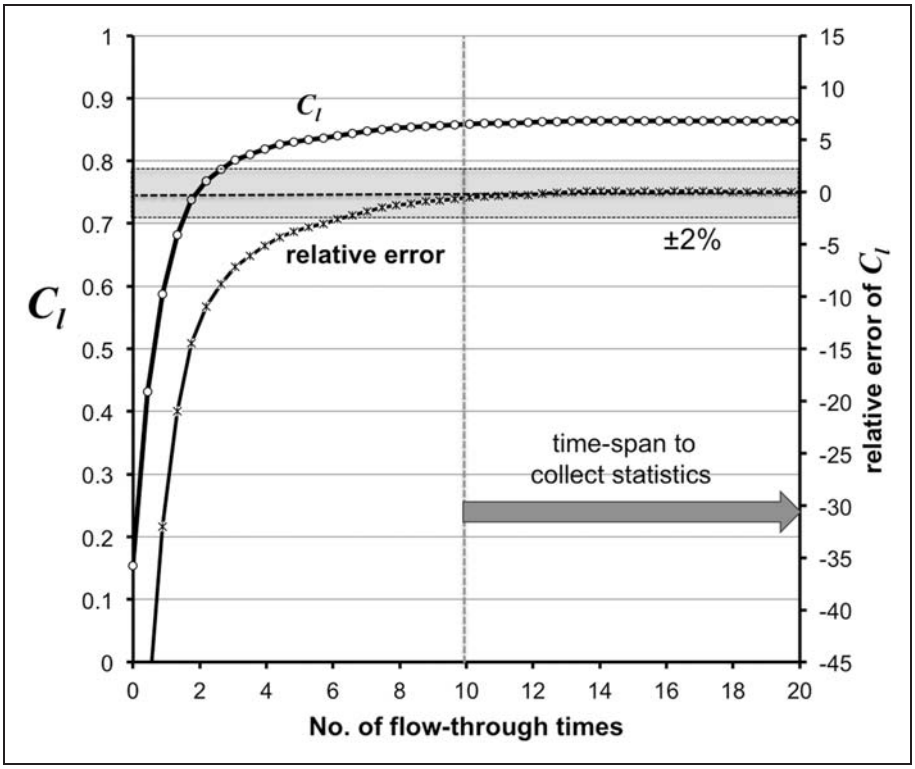

Figure 12. Evolution of lift coefficient as a function of time for the example of $\alpha = 20^\circ$. The flow is statistically steady after 10 flow-through times, and data are averaged over another 10 flow-through times.

the aircraft. Figure 12 shows the temporal evolution of the lift coefficient at $\alpha = 20^\circ$. The temporal evolution of the lift and drag coefficients during the simulation and the coefficients were within ±2% over the averaging time-span.

Numerical results

The flow visualizations show that the delta wing vortex is the main flow feature dominating the flow field (Figures 13 and 14). Figure 15 shows the contour plot of the vorticity distribution at a clip plane of $x = 200$ mm downstream of the tip of the aircraft. The vorticity distribution clearly shows the presence of the wing vortex. It can be seen that the wing vortex of the dart geometry is displaced slightly towards the wing root. This can be explained with the observation made earlier in the flow visualizations, which shows that the flow is slightly inbound towards the wing root due to the presence of the centerfold.

Figure 16 shows the vorticity intensity along a line through the vortex cores at a location $x = 200$ mm downstream of the tip of the aircraft. The vorticity indicates that the vortex of the dart is closer to the center and slightly more intense.

Next, the LES lift data are compared to literature data. Figure 17 shows the comparison of the current LES simulations of the delta wing with the measurements of Traub et al.[11] and Wentz and Kohlman.[29] The LES computations show an excellent agreement with the experiments as now the wall effects are excluded.

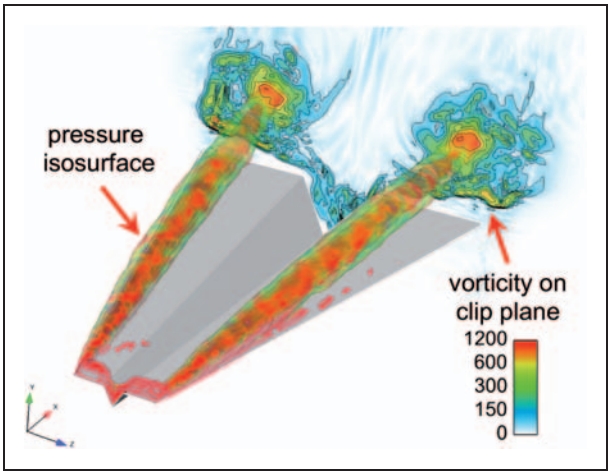

Figure 13. Instantaneous snapshot of the flow field. The pressure isosurfaces show the location of the vortex cores. The vorticity on the clip plane in the wake of the aircraft show the instantaneous nature of the flow.

Finally, the lift determined from the computational results is compared with the balance measurements in Figure 18. Generally, the agreement between experiments and computational results is good and within the experimental error of the balance. The only exception is at very high angles of attack, where the balance measurements show a higher lift due to the wall effect.

Downloaded from pig.sagepub.com at University of Sydney on March 4, 2013

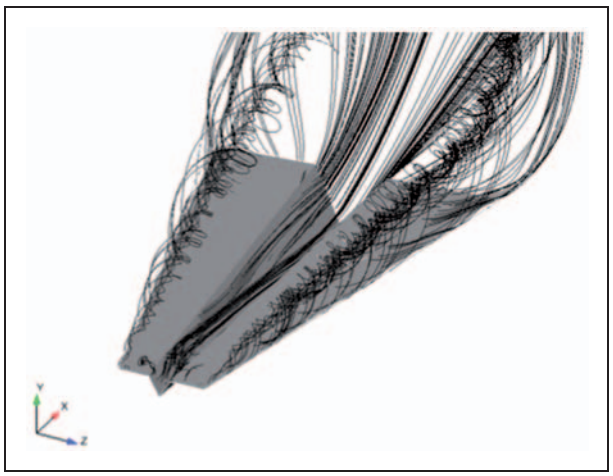

Figure 14. Time-averaged streamlines on the upper side of the airplane visualize the typical delta wing vortex at an angle of attack of $\alpha = 20^\circ$.

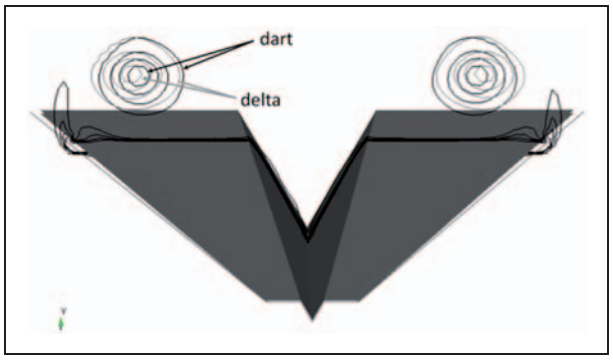

Figure 15. Contour plot of time-averaged vorticity distribution at $x = 200$ mm downstream of the tip of the aircraft. Black solid lines: vorticity contour of the dart (Model 1); gray solid lines: vorticity contours of the delta wing (Model 2); angle of attack: $\alpha = 20^\circ$.

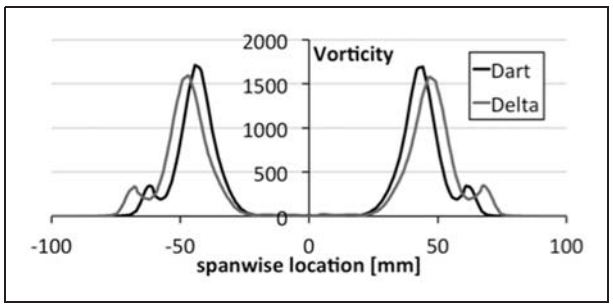

Figure 16. Vorticity distribution along a line through the vortex cores at $x = 200$ mm.

The computations confirm the trend that has been observed in the experiments, that the lift produced by the dart design with the centerfold is slightly higher than that of the delta design.

The increase of lift due to the dislocation of the wing vortex can be explained by the intensification

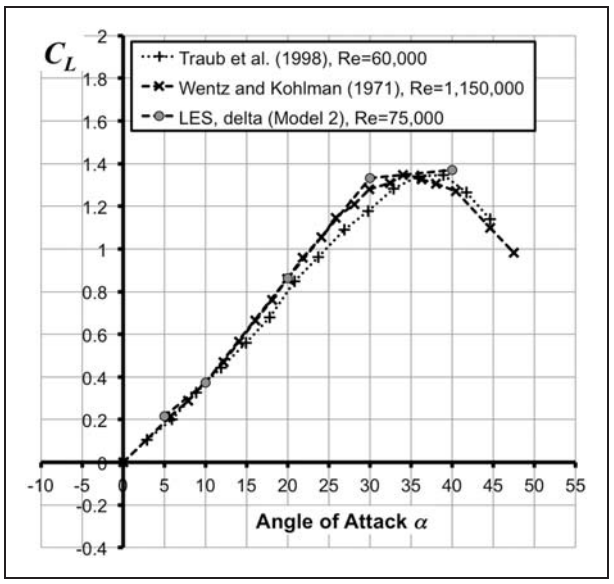

Figure 17. Lift-curve of the delta wing (Model 2) from LES results compared to literature data of Traub et al.[11] and Wentz and Kohlman.[29]
LES: large-eddy simulations.

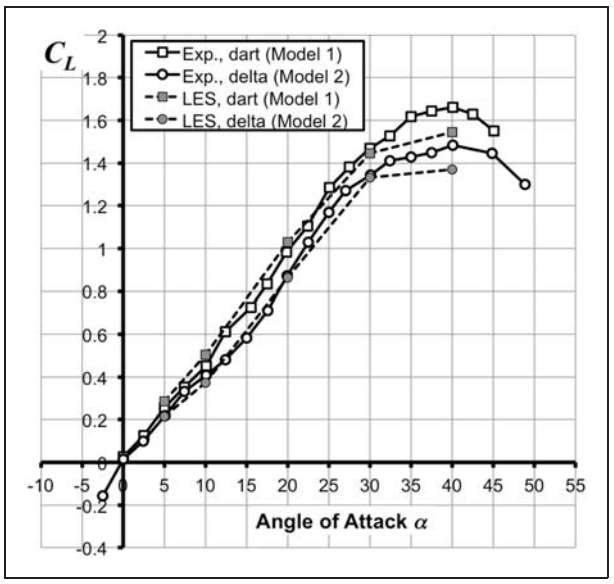

Figure 18. Comparison LES results and water tunnel measurements of model with (Model 1) and without centerfold (Model 2).

of the vortex due to the secondary flow. Celik and Roberts[30] performed experiments on a delta wing that used lateral blowing to modify the intensity of the wing vortex. Their experiments showed that lateral blowing strengthens the wing vortex and increases the normal force (the lift). The secondary flow due to the centerfold acts like the blowing mechanism of Celik and Roberts. Although the secondary flow is relatively weak compared to the blowing rates employed by Celik and Roberts, the current results show that it is strong enough to modify the wing vortex and increase the lift.

Downloaded from pig.sagepub.com at University of Sydney on March 4, 2013

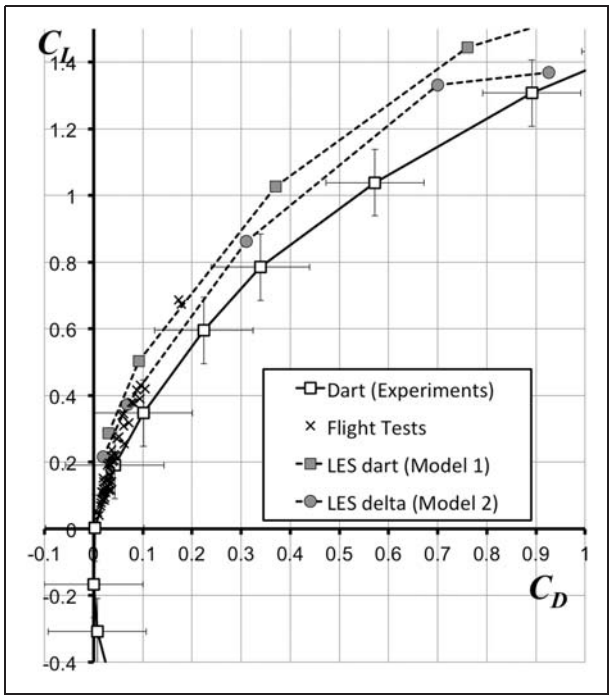

Figure 19. Comparison of lift and drag data of water tunnel experiment, flight tests[14] and simulations.

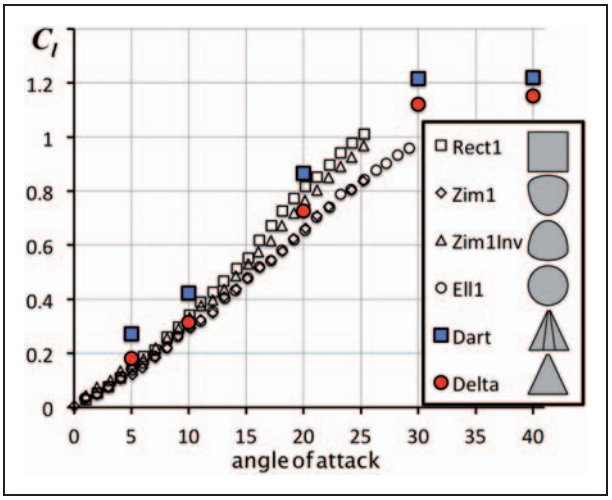

Figure 20. Comparison of lift coefficients as function of angle of attack against data from Torres and Mueller at Re = 70,000.[2] Rect1: rectangular wing; Zim1: Zimmerman shaped wing; Zim1Inv: inverse Zimmerman shaped wing; Ell1: elliptic wing.

While higher lift coefficients are desirable, the real test of an aerodynamic design lies in the lift-to-drag ratio. Figure 19 shows the lift-to-drag data of the water tunnel experiment, flight test data [14] and the simulation results. The error bars on the water tunnel results show the relatively large error, which make the current experimental results not reliable for the assessment of the lift-to-drag performance. These are included here to ascertain that the computational results are in the same order of magnitude. The same conclusion can be drawn for the flight test data. Even though there is a high uncertainty in the measurement of the lift-to-drag in flight tests, the data are in the same order of magnitude as the computations.

As the computational data showed good agreement with other experiments, the drag data of the simulations can be considered as the most accurate. The computational data shows interesting results. Generally, the lift-to-drag curve of the dart design lies to the left of the delta design, which indicates a higher aerodynamic efficiency. This demonstrates that the management of the wing vortex using a centerfold to draw the vortex inwards provides not only higher lift, but also higher lift-to-drag ratios.

Analysis

As the previous results show that the delta wing and dart configuration are promising candidates for MAV designs, the following section will compare the results from the delta wing and the dart with the aerodynamic performance of other MAV planform shapes. The data for comparison shown here are those of Torres and Mueller,[2] who have studied a variety of planform shapes in a wind tunnel at low Reynolds-number. In particular, the data for planform shapes of aspect ratio $AR = 1$ at Reynolds-number Re = 70,000 are used for the analysis here, as these resemble the current flow conditions closely.

The shapes that Torres and Mueller studied were that of a rectangular wing ('Rect1'), a so-called Zimmerman shaped wing ('Zim1'), which is formed by joining two half ellipses at the quarter-chord location, the inverse Zimmerman shaped wing ('Zim1Inv'), which is identical to the Zimmerman shaped wing, but rotated by 180°, and an elliptic wing ('Ell1').

Figure 20 compares the lift coefficients of the current computational results with the literature data. The lift coefficient of the delta wing coincides generally with the lift coefficients obtained by other planform shapes. At high angles of attack, the rectangular wing produces more lift than that of the delta wing. The dart obtains generally slightly higher lift coefficients than all other planform shapes, in particular, at low angles of attack, where other planform shapes produce a slightly non-linear lift curve.

Figure 21 compares the lift-to-drag ratios. While the lift curve shows only little sensitivity to the planform shape, the lift-to-drag ratio demonstrates larger differences. From the data of Torres and Mueller, the inverted Zimmerman shape shows high lift-to-drag ratios of over $L/\mathrm{D} > 9$. The rectangular and elliptic wing do not exceed lift-to-drag ratios of $L/D = 5$.

The delta wing and the dart show both high lift-to-drag ratios that are comparable to that of the inverted Zimmerman shape. The lift-to-drag ratio of the dart and the delta wing are very close together, which

Downloaded from pig.sagepub.com at University of Sydney on March 4, 2013

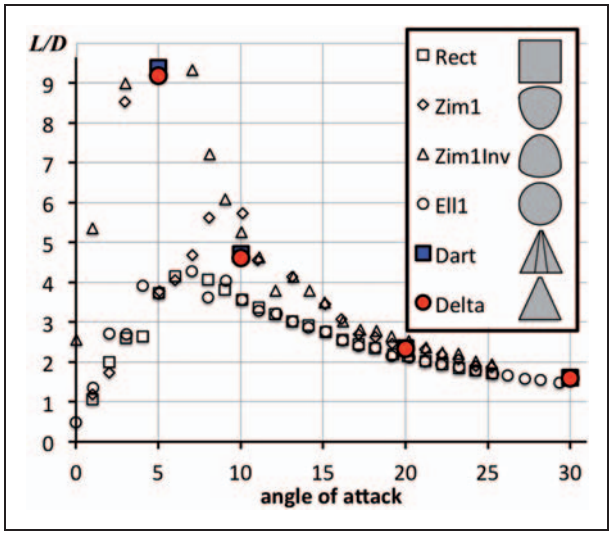

Figure 21. Comparison of lift-to-drag ratio *L/D* as function of angle of attack against data from Torres and Mueller at Re = 70,000.[2]
Rect1: rectangular wing; Zim1: Zimmerman shaped wing; Zim1Inv: inverse Zimmerman shaped wing; Ell1: elliptic wing.

means that the centerfold does not have a large influence on the aerodynamic efficiency. However, both designs, the dart and the delta wing, can both compete very well with other MAV planform shapes. It outperforms rectangular and elliptic planforms and matches that of the inverted Zimmerman. Yet, aircraft with delta wing plan forms are easier to manufacture than that with a Zimmerman shape.

Conclusions

The aerodynamic characteristics of a paper airplane have been determined to provide design recommendations for MAV. The high-sweep delta wing can obtain high lift coefficients despite having a low aspect ratio, which is a useful feature for the design of compact, sturdy MAV.

Furthermore, the centerfold of the paper airplane has been identified to alter the flow on the upper side of the wing. The centerfold creates a secondary flow that draws the wing vortex inward and leads to slightly higher lift coefficients.

This study has shown that the configuration of a typical paper airplane provides a possible layout for a MAV and promises advantages in terms of high lift capabilities and robust handling qualities. With these results, the use of high-sweep delta wings for MAV designs warrants further investigation.

Funding

This research received no specific grant from any funding agency in the public, commercial, or not-for-profit sectors.

Conflict of interest

None declared.

Acknowledgments

We thank Prof Parviz Moin and the Center for Turbulence Research for the usage of the flow solver CDP.

References

1. Mueller TJ and DeLaurier JD. An Overview of micro air vehicle aerodynamics. In: TJ Mueller (ed.) *Fixed and flapping wing aerodynamics for micro air vehicle applications*. AIAA, progress in astronautics and aeronautics, Reston, VA, USA, 2001, pp.1–10.
2. Torres GE and Mueller TJ. Aerodynamic characteristics of low aspect ratio wings at low reynolds numbers. In: TJ Mueller (ed.) *Fixed and flapping wing aerodynamics for micro air vehicle applications*. AIAA progress in astronautics and aeronautics, Reston, VA, 2001, pp.115–141.
3. Azuma A. Flight by beating. In: Schetz JA (ed) *The biokinetics of flying and swimming*. 2nd ed. Reston, Virginia: American Institute of Aeronautics and Astronautics: AIAA Education Series, 2006, pp. 123–276.
4. Shyy W. *Aerodynamics of low Reynolds number flyers*. New York: Cambridge University Press, 2008.
5. Kellogg J, Bovais C, Dahlburg J, et al., The NRL MITE Air Vehicle. In: *International conference of unmanned air vehicle systems,* 2001, Bristol, UK.
6. Grasmeyer JM and Keennon MT. Development of the black widow micro air vehicle. In: *39th AIAA aerospace sciences meeting and exhibit* 2001, Reno, NV, USA.
7. Selig MS, Guglielmo JJ, Broern AP, et al. Experiments on airfoils at low Reynolds numbers. In: *34th AIAA aerospace sciences meeting and exhibit* 1996, Reno, NV.
8. Schlüter J. Lift enhancement at low Reynolds-numbers using self-activated movable flaps. *J Aircr* 2010; 47(1): 348–351.
9. Maughmer MD and Bramesfeld G. Experimental investigation of gurney flaps. *J Aircr* 2008; 45(6): 2062–2067.
10. Traub L and Agarwal G. Aerodynamic characteristics of a gurney/jet flap at low Reynolds numbers. *J Aircr* 2008; 45(2): 424–429.
11. Traub LW and Moeller Band Rediniotis O. Low-Reynolds-number effects on delta-wing aerodynamics. *J Aircr* 1998; 35(4): 653–656.
12. Ol MV and Gharib M. Leading-edge vortex structure of nonslender delta wings at low reynolds number. *AIAA J* 2003; 41(1): 16–26.
13. Taylor G. Lift enhancement over a flexible delta wing. In: *2nd AIAA flow control conference,* 2004, Portland, OR, USA.
14. Ng BF, Kng QM, Pey YY, et al. On the aerodynamics of paper airplanes. In: *27th AIAA applied aerodynamics conference,* 2009, San Antonio, TX, USA.
15. Ellington CP, Van den Berg C, Willmott AP, et al. Leading-edge vortices in insect flight. *Nature* 1996; 384: 626–630.
16. Srygley RB and Thomas ALR. Unconventional lift-generating mechanisms in free-flying butterflies. *Nature* 2002; 420: 660–664.
17. Warrick DR, Tobalske BW and Powers DR. Aerodynamics of the hovering hummingbird. *Nature* 2005; 435: 1094–1097.

Downloaded from pig.sagepub.com at University of Sydney on March 4, 2013

18. Zhang XQ, Theissen P and Schluüter JU. A lagrangian method for the treatment of freshly cleared cells in immersed boundary techniques. *Int J Comput Fluid Dyn* 2009; 23(9): 667–670.
19. Zhang XQ, Theissen P and Schlüter JU. Towards simulation of flapping wings using immersed boundary method. *Int J Numer Methods Fluids*, 71(4): 522–536.
20. Zhang XQ and Schlüter JU. Numerical study of the influence of the Reynolds-number on the lift created by a leading edge vortex Online publication 24(6) http://dx.doi.org/10.1063/1.4718322.
21. Gursul I. Review of unsteady vortex flows over delta wings. In: *21st Applied Aerodynamics Conference,* 2003, Orlando, FL, USA.
22. Gursul I, Gordnierb R and Visbal M. Unsteady aerodynamics of nonslender delta wings. *Prog Aerosp Sci* 2005; 41: 515–557.
23. Mahesh K, Constantinescu G, Apte S, et al. Large-eddy simulations of gas turbine combustors. *Annu Res Briefs* 2001; 3–18.
24. Mahesh K, Constantinescu G and Moin P. A numerical method for large-eddy simulation in complex geometries. *J Comput Phys* 2004; 197(1): 215–240.
25. Germano M, Piomelli U, Moin, et al. A dynamic subgrid-scale eddy viscosity model. *Phys. Fluids A* 1991; 3(7): 1760–1765.
26. Schlüter J. Influence of axisymmetric assumptions on large eddy simulations of a confined jet and a swirl flow. *Int J Comput Dyn* 2004; 18(3): 177–203.
27. Schlüter JU. Static control of combustion oscillations by coaxial flows: an LES investigation. *J Propul Power* 2004; 20(3): 460–467.
28. Schlüter JU, Pitsch H and Moin P. Outflow conditions for integrated large-eddy simulation/Reynolds-averaged navier-stokes simulations. *AIAA J* 2005; 43(1): 156–164.
29. Wentz WH and Kohlman DL. Vortex breakdown on slender sharp-edged wings. *J Aircr* 1971; 8(3): 156–161.
30. Celik ZZ and Roberts L. Vortical Flow Control on a Delta Wing by Lateral Blowing. In: *32nd aerospace sciences meeting and exhibit,* 1994, AIAA: Reno, NV, USA.

Appendix

Nomenclature

AR	aspect ratio
b	wing span
C_D	drag coefficient
C_L	lift coefficient
l	length of the airplane
L	lift force
L/D	lift over drag ratio
Re	Reynolds-number ($\mathrm{Re} = U_\infty \cdot l/\nu$)
S	planform area
U_∞	airspeed
α	angle of attack
Λ	sweep angle
ρ	density
ν	kinematic viscosity

Downloaded from pig.sagepub.com at University of Sydney on March 4, 2013